

Moving Aerial Base Station Networks: Stochastic Geometry Analysis and Design Perspective

S. Enayati, H. Saeedi, H. Pishro-Nik, and H. Yanikomeroglu

Abstract

Recently, the utilization of aerial base stations (ABSs) has attracted a lot of attention. For static implementation of ABSs, it has been shown that if the ABSs are statistically distributed in a given height over a cell, according to a binomial point process (BPP), a fairly uniform coverage across the cell is achievable. However, such a static deployment exhibits a poor performance in terms of average fade duration (AFD) for the static or low speed moving users and power consumption. Therefore, considering a network of moving ABSs is of practical importance. On the other hand, once such a moving ABS network is considered, the coverage probability may not necessarily remain at an acceptable level. This paper is concerned with the design of stochastic trajectory processes such that if according to which the ABSs move, in addition to improving the AFD, an acceptable coverage profile can be obtained. We propose two families of such processes, namely spiral and oval processes, and analytically demonstrate that the same coverage as the static case is achievable. We then focus on two special cases of such processes, namely, radial and ring processes, and show that the AFD is reduced about two orders of magnitude with respect to the static case. To obtain a more practical scenario, we also consider deterministic counterparts of the proposed radial and ring processes and show that similar coverage and AFD as the stochastic case can be obtained.

S. Enayati and H. Saeedi are with ECE Department, Tarbiat Modares University, Tehran, 14115, Iran. H. Pishro-Nik is with ECS Department, University of Massachusetts, Amherst, MA, 01003, USA. H. Yanikomeroglu is with SCE Department, Carleton University, Ottawa, ON, K1S 5B6, Canada. The corresponding author is H. Saeedi, email: {hsaeedi@ieee.org}. The materiel of this paper has been presented in part at International Symposium on Information Theory (ISIT), July 2018, Vail, CO, USA [1].

I. INTRODUCTION

Thanks to the recent advances in electronics and hardware technologies, communication, embedded systems, sensor and energy storage technologies as well as carbon fiber-reinforced plastic materials [2], low cost and easy deployment, unmanned aerial systems (UASs) have become one of the most attractive candidates to support and complement the present and upcoming wireless networks in different applications ranging from data collection and environment monitoring to performing as relays and aerial base stations (ABSs) in order to enhance the network coverage and throughput [3], [4].

ABSs can be both deployed statically or mobile. Although managing a static ABS network may be more appealing, two major advantages come with a network of moving ABSs. First, it has been generally stated in the literature that moving UASs outperform fixed ones as far as the energy consumption is concerned [5]–[7]. Another benefit of having moving ABSs is the significant reduction in average fade duration (AFD). This is defined as the average time between entering a fading situation and going out of it, and directly depends on the receiver and transmitter mobility. Intuitively, moving ABSs are expected to provide shorter AFD than static ABSs. In particular, for a strictly static ABS network, a fixed user can stay in a deep fade forever [8].

Several research directions on ABSs are in place including performance analysis [5], [9]–[13], optimal positioning [14]–[20], and path planning [6], [21]–[25]. As far as performance analysis is concerned, [9] investigated the coverage and rate performance of a network using an ABS serving cellular users affected by underlaid device-to-device (D2D) users. A throughput-delay trade-off has been considered in a throughput maximum-minimum problem in [10] to optimally allocate time to several ground terminals while the ABS is moving along a certain straight line in a cyclical time division manner. Assuming an ABS that relays data between a transmitter and

receiver in a circular path, the authors of [5] considered the variable rate protocol implementation to both the transmitter-relay and relay-receiver links in order to investigate outage probability and achievable rate. Furthermore, using the tools from the stochastic geometry, [11] and [13] provided coverage and throughput analysis in a Binomial point process (BPP) and Poisson point process (PPP) modeled networks of static ABSs, respectively. Also, [26] proposed a stochastic model for ABS networks which considers both the ABS-user link and the ABS-backhaul link simultaneously.

In papers considering the optimal deployment, the goal is often to optimize the placement of the ABSs to provide satisfaction in a variety of quality of service (QoS) levels. In this regard, [14] optimizes the distance between two ABSs in two cases of having and not-having interference to obtain a certain coverage probability in a given area. In [15], assuming only a line-of-sight (LoS) dominated channel, simulation based sequential algorithms have been presented to obtain the minimum number of ABSs and their placement to cover a given area. In a similar work, [16] obtained the minimum number and the optimal 3D placement of the ABSs using the particle swarm optimization (PSO) algorithm. The authors in [17] optimized the 3D location of multiple ABSs using circle packing theory that led to a maximum coverage and minimum transmit power for the ABSs. The same authors in [18] and [19] proposed a cell association algorithm using the optimal transport theory while considering the terrestrial base stations in the latter.

As the mobility is the unique feature of the ABSs compared to their counterpart, i.e., terrestrial base stations, it is not surprising that many studies have recently been devoted to this aspect. In particular, path planning problems have been proposed in which, similar to the previous category, the goal is to design an optimal path to satisfy certain QoS indicators. In [6] after deriving a theoretical model for the propulsion energy consumption, the authors investigated the energy efficiency problem in a certain circular trajectory and a general trajectory of a single

ABS. Movement minimization of data collecting ABSs to obtain the optimum trajectory was considered in [21], where the authors are also willing to make the power transmission of Internet of things (IoT) devices more efficient. In [22], the user scheduling and a single ABS trajectory were jointly optimized with the objective of maximizing the minimum average sum rate. A similar idea was considered in [23] for the multi-ABS case. A recent trajectory planning was investigated in [24] in which a single UAV is considered to help a ground BS while turning a circular path around it with a constant speed. A similar trajectory was considered in [25], where for a multiple antenna equipped UAV, the transmission duration and the transmit power were jointly optimized to obtain the maximum data collection efficiency.

As can be seen, many works have dealt with moving ABSs, most of which deal with finding optimal trajectory paths with different utility functions such as sum-rate or energy efficiency, e.g., [6], and [21]–[25], [27]. However, there is no work in multi UAV network in the literature that uses coverage probability as the utility function as it can result in intractable and complicated optimization problems. Moreover, even for deterministic utility functions, the optimization problems are sometimes so complicated to solve that many works investigate a network with a single ABS [22], [24], [25], [28]–[31] and in many cases, it is assumed that we know the locations of the users and/or other elements of the network, e.g., [31], [32]–[34]. In this paper, we aim to present a different perspective on the motion analysis of the ABSs. Our scheme makes it possible to deal with probabilistic measures such as coverage probability and there is no limitation in analyzing multiple ABSs and mobile users. Such a stochastic analysis has been applied widely to several cellular network frameworks, see, e.g., [35]–[37] and references therein.

As far as ABS networks are concerned, stochastic geometry analysis has already been applied to a network of fixed ABSs [11]. In this work, the ABSs are modeled according to a uniform BPP

and then the closed-form formulations for coverage probability are obtained. Analysis shows that such a BPP distribution for ABSs can provide fairly uniform coverage across the cell and the outage probability can be maintained below an acceptable value throughout the cell. However, if the ABSs are assumed to be moving, this is not the case anymore necessarily. For example, let's assume ABSs start their flight with constant speed from the cell center towards the cell edge in straight lines with an angle uniformly chosen with respect to the X axis and return on the same line before they choose a new angle and leave the origin again at another random angle. This can be seen as one of the simplest trajectories that comes to mind. After few departures/arrivals from/to the origin, this moving pattern leads ABSs to be concentrated at the cell center which results in the coverage probability degradation at the cell edge. In Fig. 1, we have compared the coverage profile resulting from the considered moving pattern to the coverage obtained by deploying BPP-distributed static ABSs. As can be seen, the coverage probability at the cell edge is not acceptable for the moving case.¹

In this paper, our aim is to design a family of trajectory processes that if according to which the ABSs move, a fairly uniform user coverage can be maintained while taking advantage of the benefits of ABS mobility. The results are promising: we analytically demonstrate that the proposed family of trajectory processes can maintain the same coverage behavior as that of the uniform BPP. Through simulation, we observe significant improvement in the AFD compared to the static case. This is in addition to the saving we obtain in energy consumption as stated in the literature².

The obtained stochastic trajectory curves are then used as a building block to design determin-

¹In addition to the results of the figure, the non-uniformity of the points in the case of constant speed can be proved analytically. We have not stated the proof here due to space limitation.

²This statement regarding the energy comes from [5]–[7] and is not simulated in this paper.

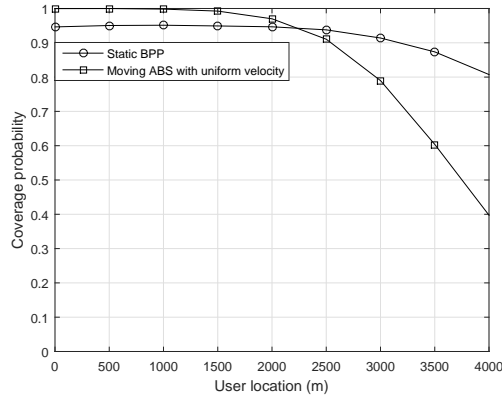


Fig. 1. Coverage probability vs. distance to origin for a cell with radius $\rho = 4$ km and 10 ABSs. For static case, ABSs are distributed according to BPP. For the mobile case, the ABSs move with a constant speed of 5 m/s.

istic trajectory curves that are practically implementable. We show that with reasonable number of ABSs, we can obtain similar AFD and coverage probability as that of the stochastic case without the ABSs being moving in stochastic paths.

This paper is organized as follows: in Section II, we revisit some existing definitions and formulations for coverage probability in a finite network of ABSs. In Section III, we introduce two general family of stochastic trajectory processes and their corresponding special cases as well as the deterministic design. Section IV provides simulation results and Section V concludes the paper.

Notations: In this paper, deterministic quantities are denoted by italic letters, while stochastic quantities are denoted by bold-face lower-case and upper-case letters.

II. SYSTEM MODEL AND PRELIMINARIES

In this section, we review the concept of general BPP and uniform BPP. Then, we explain the system model and review the formulations for the coverage probability corresponding to a network in which the ABSs are modeled as a BPP. If a fixed number of points are independently

and identically distributed (i.i.d.) on a compact set $W \in R^d$ [38], we say the points can be modeled as a general BPP. If these points are distributed uniformly within the same compact set, then we say the points are modeled according to a uniform BPP .

Now suppose that N ABSs at height H are distributed according to a BPP in a circle with radius of ρ and start their flights independently following an arbitrary trajectory process, $\{\mathbf{X}_1(t), \mathbf{X}_2(t), \mathbf{X}_3(t), \dots\}$, at times $\mathbf{T}_1, \mathbf{T}_2, \dots, \mathbf{T}_N$, chosen uniformly and independently from $(0, \tau)$, respectively, according to a given PDF (it is assumed that the trajectory curves are chosen independently from a certain probability space, and are independent from the starting times $\mathbf{T}_1, \mathbf{T}_2, \dots, \mathbf{T}_N$). It can be easily seen that at any arbitrary observation time of $t' \geq \tau$, the ABSs still follow a general BPP. However, if these ABSs are distributed according to uniform BPP and move according to an arbitrary trajectory, at a given time instant, then ABSs do not necessarily follow a uniform BPP model.

We assume that N ABSs are BPP-distributed at the fixed height of H above a circular area of radius ρ , referred to as cell³. The ABSs can be static or moving. At any time snapshot, the aim is to provide coverage for the user located at a given point $(x_0, 0, 0)$. We assume that the user is connected to its closest ABS, called the serving ABS where the instantaneous distance between the serving ABS and the user is denoted by r . Note that in a dynamic network, the user can be handed over to a different ABS based on the change in the value of r . Assuming ABSs share the same resource blocks in time or frequency with a reuse factor of 1, the other ABSs are considered as interfering ABSs. Alternatively, we can assume that the spectrum is divided between the ABS's.

Using the formulation of [11] for the case of uniform BPP, we can revisit the following proposition corresponding to the coverage probability for the case of uniform BPP:

³In this paper by cell, we mean a circular area without any ground base stations that aims to be covered by a set of ABSs.

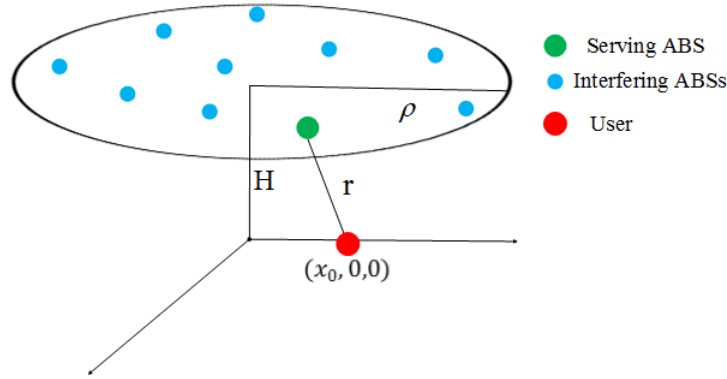


Fig. 2. N Static ABSs scattered uniformly in a circular cell at the height of H .

Proposition 1. *If the ABSs are modeled as a uniform BPP, coverage probability of a typical user located at $(x_0, 0, 0)$, assuming a Nakagami- m fading channel model is obtained from the following formulation [11]:*

$$P_c = \int_H^{w_m} \left(\sum_{k=0}^{m_0-1} \frac{(-s)^k}{k!} \left[\frac{\partial^k}{\partial s^k} A(s, r, x_0) \Big|_{s=m_0 \beta r^\alpha} \right] \right) N (1 - F_{W_{i,1}}(r|x_0))^{N-1} f_{W_{i,1}}(r|x_0) dr$$

$$+ \int_{w_m}^{w_p} \left(\sum_{k=0}^{m_0-1} \frac{(-s)^k}{k!} \left[\frac{\partial^k}{\partial s^k} B(s, r, x_0) \Big|_{s=m_0 \beta r^\alpha} \right] \right) N (1 - F_{W_{i,2}}(r|x_0))^{N-1} f_{W_{i,2}}(r|x_0) dr. \quad (1)$$

In (1), $A(s, r, x_0)$ and $B(s, r, x_0)$ are the obtained by:

$$A(s, r, x_0) = \left[\int_r^{w_m} \left(1 + \frac{s u_i^{-\alpha}}{m} \right)^{-m} \frac{f_{W_{i,1}}(u_i|x_0)}{1 - F_{W_{i,1}}(r|x_0)} du_i \right.$$

$$\left. + \int_{w_m}^{w_p} \left(1 + \frac{s u_i^{-\alpha}}{m} \right)^{-m} \frac{f_{W_{i,2}}(u_i|x_0)}{1 - F_{W_{i,1}}(r|x_0)} du_i \right]^{N-1},$$

and

$$B(s, r, x_0) = \left[\int_r^{w_p} \left(1 + \frac{s u_i^{-\alpha}}{m} \right)^{-m} \frac{f_{W_{i,2}}(u_i|x_0)}{1 - F_{W_{i,2}}(r|x_0)} du_i \right]^{N-1},$$

respectively, where $F_{W_{i,1}}(r|x_0)$ and $F_{W_{i,2}}(r|x_0)$ are the cumulative distribution functions (CDF)s of the distances from the receiver to the ABSs denoted by $\{W_i\}$ conditioned on x_0 given as below:

$$F_{W_{i,1}}(r|x_0) = \frac{r^2 - H^2}{\rho^2},$$

$$F_{W_{i,2}}(r|x_0) = \frac{r^2 - H^2}{\pi\rho^2} (\theta^* - 0.5 \sin 2\theta^*) + \frac{1}{\pi} (\phi^* - 0.5 \sin 2\phi^*),$$

where

$$\theta^* = \arccos\left(\frac{r^2 + x_0^2 - d^2}{2x_0\sqrt{r^2 - H^2}}\right),$$

and

$$\phi^* = \arccos\left(\frac{x_0^2 + d^2 - r^2}{2x_0\rho}\right).$$

Also, $f_{W_{i,1}}(u_i|x_0)$ and $f_{W_{i,2}}(u_i|x_0)$ are the set of distance probability distribution functions (PDF)s of ABSs conditioned on x_0 given by:

$$f_{W_{i,1}}(u_i|x_0) = \frac{2u_i}{\rho^2},$$

and

$$f_{W_{i,2}}(u_i|x_0) = \frac{2u_i}{\pi\rho^2} \arccos\left(\frac{u_i^2 + x_0^2 - d^2}{2x_0\sqrt{u_i^2 - H^2}}\right).$$

Furthermore, $w_m = \sqrt{(\rho - x_0)^2 + H^2}$, $w_p = \sqrt{(\rho + x_0)^2 + H^2}$, and $d = \sqrt{\rho^2 + H^2}$, β is the signal-to-interference ratio (SIR) threshold, $\alpha > 2$ is the path-loss exponent, and m_0 and m are the Nakagami- m parameters of the serving and interfering links, respectively. A key feature of ABSs is their ability to change altitude. However, considering this extra degree of freedom adds to the complexity of an already involved design problem. Therefore, in this paper, we assume all ABSs fly in a fixed altitude. Also, in most countries, the existing policies impose important restrictions to the height and UAV may end up flying at a limited range altitude.

III. STOCHASTIC TRAJECTORY PROCESSES THAT PROVIDE UNIFORM COVERAGE

A. General Idea and Summary of Results

In the previous section, we reviewed the result of [11] in which for a network of static ABSs modeled according to uniform BPP, closed-form formulations for coverage were obtained. As shown in Fig. 1, such a distribution provides fairly uniform coverage across the cell but as long as the ABSs are static, the user experience in terms of AFD is poor. In the same figure, we observed that if the ABSs start moving, while the AFD experience may improve, such a uniformity in coverage is not necessarily preserved. Therefore in this section, we are looking for trajectory processes such that if according to which the ABSs move, the points remain to follow BPP at any time instant, leading to an almost uniform coverage. So far, we have been able to identify two families of such trajectory processes, referred to as *spiral* and *oval* trajectory processes.

Before getting involved with the detailed analytical formulations and their derivations, we provide an intuitive summary first. As mentioned above, we have identified two major families of processes, namely, spiral and oval. In spiral trajectory processes, each ABS generally starts flying from the cell origin towards the cell edge according to the specs itemized in Definition 1 of the next subsection. An important member of this family is called the radial trajectory process in which the trajectories are in fact the cell radius. In oval trajectory processes, each ABS moves on a closed curve, containing the cell origin within it according to the specs itemized in Definition 2 of the next subsection. An important member of this family is called the ring trajectory process in which the trajectories are in fact randomly-selected cell radii, all centered at the cell origin.

An important question that may arise is how to implement such stochastic moving paths in a deterministic way. To address this question, by focusing on the radial and ring trajectory

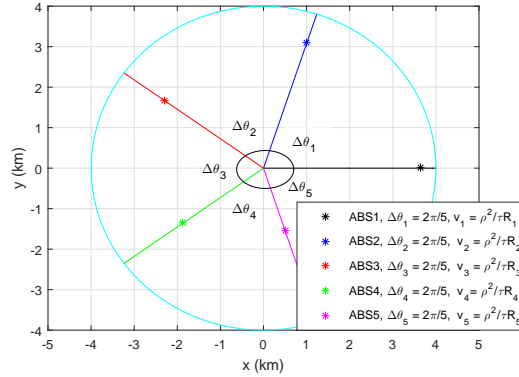


Fig. 3. ABSs location according to deterministic radial trajectory in a cell of radius 4 km.

processes, we introduce their deterministic counterparts and show that they also provide similar behavior in terms of coverage and AFD to the stochastic case.

For the deterministic radial trajectory, we claim that we can achieve the required uniform coverage with N available ABSs across a cell of radius ρ , if they are scheduled to move as follows:

- 1- For an arbitrary initial phase β , the i th ABS will fly on a radius with phase $\beta + 2\pi(i-1)/N$.
- 2- For an arbitrary constant value τ , all ABSs fly with similar speed profiles, $v_i = \frac{\rho^2}{R_i \tau}$, where R_i is the instantaneous distance to the origin.
- 3- The i th ABS departs origin at time $i\tau/(N+1)$.
- 4- Once any ABS reaches the edge of the cell, it reverses its direction and returns to the origin with the same speed profile as in Item 2 and this cycle continues periodically.

Fig. 3 shows a snapshot of the ABSs' coordinates in a cell with radius of 4 km, for $N = 5$.

For the deterministic ring trajectory, we claim that we can achieve the required uniform coverage with N available ABSs across a cell of radius ρ , if they are scheduled to move as follows:

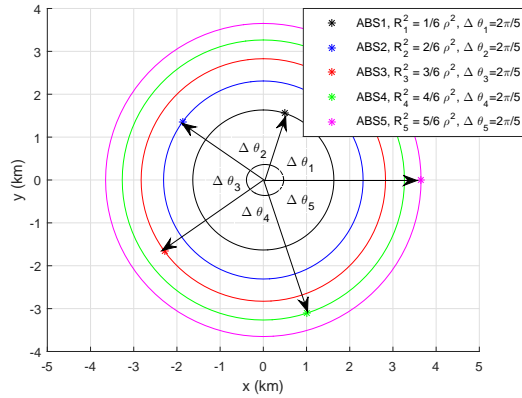


Fig. 4. ABSs location according to deterministic ring trajectory in a cell of radius 4 km.

1- The i th ABS will fly on circle with radius $R_i = \sqrt{\frac{i}{N+1}}\rho$.

2- The i th ABS has to turn around the center every τ seconds with constant speed of $v_i = 2\pi R_i/\tau$ where τ is an arbitrary constant.

3-The i th ABS has to have instantaneous phase of $\phi + 2\pi i/N$ where ϕ is a constant depending on the time we take the snapshot of the network.

4- It can be easily seen that all ABSs fly with equal angular speeds and therefore, the phase difference of $2\pi/N$ is preserved at any time instant.

Fig. 4 shows a snapshot of the ABSs' coordinates for $N = 5$ in a cell with radius of 4 km.

For both cases, by changing the value of τ , we can control the moving speed of the ABSs. In the rest of this section, we will provide the details on spiral and oval trajectory processes and their special cases, i.e., radial and ring processes and then we will prove our above claims, indicating that the 2 suggested deterministic schemes can provide a coverage profile similar to the static case reported in Fig. 1.

B. Spiral Trajectory Processes

1) *General Concept:* For $\underline{c} = (c_x, c_y) \in \mathbb{R}^2$, let $B(\underline{c}, \rho) = \{(x, y) \in \mathbb{R}^2 : (x - c_x)^2 + (y - c_y)^2 \leq \rho^2\}$. Let also $\underline{Q} = (0, 0)$. Then we state the following definition:

Definition 1. Let $\underline{X}(s) : [0, 1] \mapsto B(\underline{Q}, \rho)$ be twice differentiable curves, $\underline{X}(s) = (x(s), y(s))$, with the following properties:

(a) $\underline{X}(0) = \underline{Q}$, $x(1)^2 + y(1)^2 = \rho^2$;

(b) $r(s) \triangleq \sqrt{x(s)^2 + y(s)^2}$ is a strictly increasing function of s for all $s \in [0, 1]$.

Now for any $\tau > 0$, define the mappings $h : [0, 1] \mapsto [0, \tau]$ as $h(s) = \frac{\tau r(s)^2}{\rho^2}$. Suppose that N aerial vehicles start their flights at times $\mathbf{T}_1, \mathbf{T}_2, \dots, \mathbf{T}_N$, independently chosen uniformly from $(0, \tau)$. For $k\tau + \mathbf{T}_i \leq t \leq (k+1)\tau + \mathbf{T}_i$, we define the **spiral trajectories** $\tilde{\mathbf{X}}_i(t) = (\tilde{\mathbf{x}}_i(t), \tilde{\mathbf{y}}_i(t))$ for the i 'th vehicle as

$$(\tilde{\mathbf{x}}_i(t), \tilde{\mathbf{y}}_i(t)) = \begin{cases} ROT_{\Theta_i} \left(x_i(h_i^{-1}(t - k\tau - \mathbf{T}_i)), y_i(h_i^{-1}(t - k\tau - \mathbf{T}_i)) \right), & k \text{ even} \\ ROT_{\Theta_i} \left(x_i(h_i^{-1}((k+1)\tau + \mathbf{T}_i - t)), y_i(h_i^{-1}((k+1)\tau + \mathbf{T}_i - t)) \right), & k \text{ odd,} \end{cases} \quad (2)$$

where ROT_{Θ_i} is the rotation around the origin by Θ_i degrees where $\Theta_i \sim U(0, 2\pi)$ are chosen independently when the vehicle starts its departure from the origin.

In order to have a better insight of the curves satisfying Properties (a) and (b), we provide a family of general curves here. Assume that

$$\underline{X}(s) = [\rho s^k \cos(\zeta s), \rho s^k \sin(\zeta s)], \quad s \in [0, 1], \quad (3)$$

where depending on the values of ρ , k and ζ , different curves can be generated. For example, by setting $\rho = 5$, $k = 2$ and $\zeta = 2\pi$ we obtain curves in Fig. 5 where $X_2(s) = -X_1(s)$. Now before proposing Theorem 1, let's state the following lemma which will be used later in the proof of Theorem 1 :

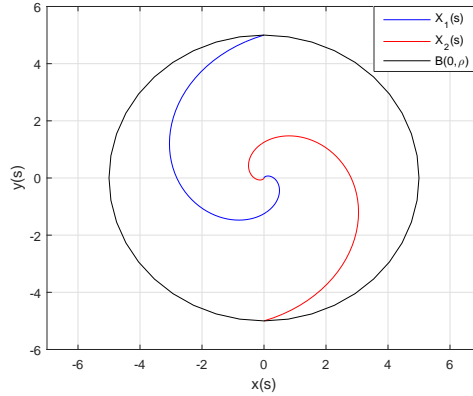


Fig. 5. Typical curves from the spiral trajectory process with $\rho = 5$, $k = 2$ and $\zeta = 2\pi$.

Lemma 1. Consider a periodic function $g : \mathbb{R} \mapsto [0, \infty)$, where $g(t+\tau) = g(t), \forall t \in \mathbb{R}$. $F_{\mathbf{R}(t)}(r)$, the CDF of the randomly shifted process $\mathbf{R}(t) \triangleq g(t - \mathbf{T}), \mathbf{T} \sim U(0, \tau)$, is obtained by

$$F_{\mathbf{R}(t)}(r) = \frac{|\mathcal{A}|}{\tau}, \quad (4)$$

where $|\cdot|$ is the Lebesgue measure of \mathcal{A} defined as $\mathcal{A} = \{\alpha \in [0, \tau] \mid g(\alpha) \leq r\}$.

Proof.

$$\begin{aligned} F_{\mathbf{R}(t)}(r) &= \int_0^\tau \Pr(g(t - \mathbf{T}) \leq r \mid \mathbf{T} = \alpha) f_{\mathbf{T}}(\alpha) d\alpha \\ &= \frac{1}{\tau} \int_0^\tau 1_{\{g(t-\alpha) \leq r\}} d\alpha = \frac{|\mathcal{A}|}{\tau}, \end{aligned} \quad (5)$$

where \mathcal{A} is defined as the region in which $g(\alpha) \leq r$ during one period, i.e., $\mathcal{A} = \{\alpha \in [0, \tau] \mid g(\alpha) \leq r\}$. \square

Corollary 1. If we have $g(2\tau - t) = g(t), t \in (0, \tau)$, and $\mathbf{R}(t) \triangleq g(t - \mathbf{T}), \sim U(0, \tau)$, we get a similar distribution since $g(t)$ is symmetric with respect to τ .

Now we are ready to state the following theorem:

Theorem 1. For all $t > \tau$, the instantaneous locations of the aerial vehicles on the spiral trajectory, i.e., $\tilde{\mathbf{X}}_i(t) = (\tilde{\mathbf{x}}_i(t), \tilde{\mathbf{y}}_i(t))$, form a uniform BPP in $B(\underline{Q}, \rho)$.

Proof. For the proof of Theorem 1, we first need to show that for $t \geq \tau$, the location of vehicles are independent. This is intuitive, since $\Theta_i \sim U(0, 2\pi)$ and $\mathbf{T}_i \sim U(0, \tau)$ both have been chosen independently. Second, we have to show that the locations are uniformly distributed in $B(\underline{Q}, \rho)$. To do so, we note that since $\Theta_i \sim U(0, 2\pi)$, the phase of an arbitrary point on the curve is uniformly distributed between 0 and 2π , i.e., $\angle \tilde{\mathbf{X}}_i(t) \sim U(0, 2\pi)$. It only remains to show that the CDF of the distance between the origin and an arbitrary point on the curve, i.e., $\|\tilde{\mathbf{X}}_i(t)\|$, is equal to the distribution corresponding to uniform BPP within $B(\underline{Q}, \rho)$. For notational simplicity, we drop index i in the rest of the proof.

Let

$$u(t) \triangleq \begin{cases} \|X(h^{-1}(t))\| & 0 \leq t \leq \tau \\ \|X(h^{-1}(2\tau - t))\| & \tau \leq t \leq 2\tau \end{cases}. \quad (6)$$

We provide the proof for the case of $0 \leq t \leq \tau$, the proof for the case of $\tau \leq t \leq 2\tau$ is similar.

According to (6) and Property 2 in Definition 1, we understand that

$$u(t) = \|X(h^{-1}(t))\| = r(h^{-1}(t)). \quad (7)$$

Also, since the random rotation of $X(t)$ will not affect its absolute value, we have $\|\tilde{\mathbf{X}}(t)\| = u(t - \mathbf{T})$ where $\tilde{\mathbf{X}}(t)$ is the randomly rotated and shifted version of $X(t)$ defined in Eq. (2).

Now using Lemma (1), we obtain $F_{\|\tilde{\mathbf{X}}\|}$ as below

$$\begin{aligned} F_{\|\tilde{\mathbf{X}}\|} &= \frac{1}{\tau} |\{0 \leq \alpha \leq \tau : u(\alpha) \leq r\}| \\ &= \frac{1}{\tau} |\{0 \leq \alpha \leq \tau : \|X(h^{-1}(\alpha))\| \leq r\}|. \end{aligned} \quad (8)$$

Again, according to Property 2, since $r(s)^2$ is strictly increasing, $h(s) = \frac{\tau r(s)^2}{\rho^2}$ is also strictly increasing and hence, there exists an α_{\max} such that

$$\|X(h^{-1}(\alpha_{\max}))\| \leq r. \quad (9)$$

Therefore, $F_{\|\tilde{\mathbf{X}}\|} = \frac{|[0, \alpha_{\max}]|}{\tau} = \frac{\alpha_{\max}}{\tau}$. Now suppose there exists an arbitrary $0 \leq \alpha^* \leq \tau$ such that

$$\alpha^* = \frac{\tau r^2}{\rho^2}. \quad (10)$$

This means there exists a $s^* \in [0, 1]$ such that

$$\alpha^* = h(s^*) = \frac{\tau r^{*2}}{\rho^2}, \quad (11)$$

which means $r^* = r(h^{-1}(\alpha^*)) = r$. Therefore, we have

$$h^{-1}(\alpha^*) = h^{-1}(\alpha_{\max}), \quad (12)$$

according to (9). By this, we can uniquely obtain $\alpha^* = \alpha_{\max}$, since h is monotonic. Finally, the CDF can be written as

$$F_{\|\tilde{\mathbf{X}}\|} = \frac{|\{0 \leq \alpha \leq \alpha_{\max}\}|}{\tau} = \frac{r^2}{\rho^2}, \quad (13)$$

which is the same as the CDF corresponding to a BPP within $B(\underline{Q}, \rho)$. This completes the proof. \square

The family of curves introduced by this theorem is quite diverse. In the next subsection, we focus on one of the simple trajectory processes of this family called radial trajectory process.

2) *Radial Trajectory Process*: A sample radial trajectory process is shown in Fig. 6. It can be obtained by setting $k = 1$ and $\zeta = 0$ in (3). In this setup, we consider a cell with radius ρ . We assume that N ABSs start to take off from the cell center at random moments $\mathbf{T}_1, \mathbf{T}_2, \dots, \mathbf{T}_N \in (0, \tau)$ where τ is the initialization time in which all N ABSs start to take off. $\mathbf{T}_1, \mathbf{T}_2, \dots, \mathbf{T}_N$ are independently chosen uniformly from $(0, \tau)$. Each ABS first flies to a

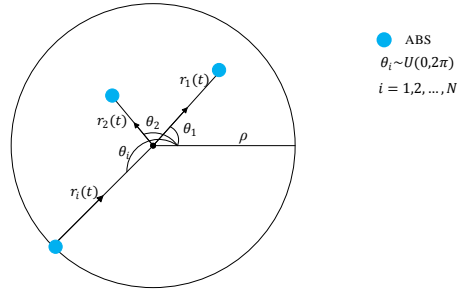


Fig. 6. An illustration of flying ABSs according to a radial trajectory process.

predetermined altitude of H and then chooses a random angle $\Theta_i \in (0, 2\pi)$ uniformly and flies in a straight line towards the cell edge where its distance to origin at time t is shown by the random variable $\mathbf{R}(t)$. When an ABS reaches the cell edge, it returns to the origin on the same angle to complete the first cycle and this action repeats continuously. For each half cycle $k\tau + \mathbf{T}_i \leq t \leq (k+1)\tau + \mathbf{T}_i$, $\mathbf{R}(t)$ has to satisfy the following formulation:

$$\mathbf{R}_i(t) = \begin{cases} \rho \sqrt{\frac{t - \mathbf{T}_i - k\tau}{\tau}}, & k \text{ even} \\ \rho \sqrt{\frac{(k+1)\tau + \mathbf{T}_i - t}{\tau}}, & k \text{ odd} \end{cases}. \quad (14)$$

Note that with this definition, we have $\mathbf{R}_i(k\tau) = 0$ if k is even and $\mathbf{R}_i(k\tau) = \rho$ otherwise. In other words, τ is the time it takes for an ABS to go from center to the edge. It is worth mentioning that during the initial take off phase, it takes a while for each ABS to get to the altitude H , but we assume this time is negligible compared to τ . By the description above, one can understand that after the time τ , we have N ABSs flying at the altitude of H .

A very interesting point in radial trajectory process is the behaviour of the ABS velocity which

can be obtained by the taking derivative of (14):

$$\mathbf{V}_i(t) = \begin{cases} \frac{\rho}{\sqrt{\tau(t-\mathbf{T}_i-k\tau)}}, & k \text{ even} \\ -\frac{\rho}{\sqrt{\tau((k+1)\tau+\mathbf{T}_i-t)}}, & k \text{ odd} \end{cases}. \quad (15)$$

Eq. (15) demonstrates that as t increases (i.e., ABS is at larger distance from the center), its velocity decreases which means that it spends longer time flying at the larger distances to provide a uniform coverage.

C. Oval Trajectory Processes

1) General Concept:

Definition 2. For any given $a, b \in \mathbb{R}^+$, where $0 \leq a \leq b \leq \rho$, let $\underline{X}^{a,b}(s) : [0, 1] \mapsto B(\underline{Q}, \rho)$ be twice differentiable curves, $\underline{X}^{a,b}(s) = (x_1^{a,b}(s), x_2^{a,b}(s))$, with the following properties:

- (a) $\underline{X}^{a,b}(0) = (0, a)$, $\underline{X}^{a,b}(1) = (b, 0)$;
- (b) $r^{a,b}(s) \triangleq \|\underline{X}^{a,b}(s)\| = \sqrt{x_1^{a,b}(s)^2 + x_2^{a,b}(s)^2}$ is a non-decreasing function of s for all $s \in [0, 1]$.

Now, for any $\tau > 0$, define the mappings $h_{a,b} : [0, 1] \mapsto [0, \frac{\tau}{4}]$ as

$$h^{a,b}(s) = \frac{\tau(r^{a,b}(s) - a)}{4(b - a)}. \quad (16)$$

In addition, for $i \in \{1, 2, \dots, N\}$, assume that random variables $(\mathbf{A}_i, \mathbf{B}_i)$ are chosen independently according a two-dimensional probability distribution that satisfies $P(0 \leq \mathbf{A}_i \leq \mathbf{B}_i \leq \rho) = 1$ and

$$\mathbb{E}_{\mathbf{A}_i, \mathbf{B}_i} \left[\frac{1_{(\mathbf{A}_i \leq r \leq \mathbf{B}_i)}}{\mathbf{A}_i - \mathbf{B}_i} \right] = \frac{2r}{\rho^2}, \quad \text{for all } r \in [0, \rho]. \quad (17)$$

We define the corresponding **oval trajectories** $\underline{Z}^{a,b}(t) : [0, \tau] \mapsto B(\underline{O}, \rho)$ as in Equations (18)

and (19), for $0 \leq t \leq \frac{\tau}{2}$ and $\frac{\tau}{2} \leq t \leq \tau$, respectively:

$$\underline{Z}^{a,b}(t) = (z_1^{a,b}(t), z_2^{a,b}(t)) = \begin{cases} \left(x_1^{a,b}(h_i^{-1}(t)), x_2^{a,b}(h_i^{-1}(t)) \right), & \text{for } 0 \leq t \leq \frac{\tau}{4} \\ \left(-x_1^{a,b}(h_i^{-1}(\frac{\tau}{2} - t)), x_2^{a,b}(h_i^{-1}(\frac{\tau}{2} - t)) \right), & \text{for } \frac{\tau}{4} \leq t \leq \frac{\tau}{2} \end{cases}, \quad (18)$$

$$\underline{Z}^{a,b}(t) = (z_1^{a,b}(t), z_2^{a,b}(t)) = \begin{cases} \left(-x_1^{a,b}(h_i^{-1}(t - \frac{\tau}{2})), -x_2^{a,b}(h_i^{-1}(t - \frac{\tau}{2})) \right), & \text{for } \frac{\tau}{2} \leq t \leq \frac{3\tau}{4} \\ \left(x_1^{a,b}(h_i^{-1}(\tau - t)), -x_2^{a,b}(h_i^{-1}(\tau - t)) \right), & \text{for } \frac{3\tau}{4} \leq t \leq \tau \end{cases}. \quad (19)$$

Now for any ABS i , we set $a = \mathbf{A}_i$ and $b = \mathbf{B}_i$ to generate $Z_i^{a,b}(t)$. The **extended oval trajectories**,

$\underline{\tilde{Z}}^{a,b}(t) = (\tilde{z}_1^{a,b}(t), \tilde{z}_2^{a,b}(t)) : \mathbb{R}^+ \mapsto B(\underline{O}, \rho)$, are defined by periodically extending $\underline{Z}^{a,b}(t)$ outside of $[0, \tau]$ such that

$$\underline{\tilde{Z}}^{a,b}(t + \tau) = \underline{\tilde{Z}}^{a,b}(t), \quad \text{for } t \in \mathbb{R}^+.$$

Suppose that N aerial vehicles start their flights at times $\mathbf{T}_1, \mathbf{T}_2, \dots, \mathbf{T}_N$, independently chosen uniformly from $(0, \tau)$. Let also $\underline{\mathbf{W}}_i^{\mathbf{A}_i, \mathbf{B}_i}(t)$ be the corresponding **delayed extended oval trajectories** according to \mathbf{T}_i 's, i.e., for $t \in [\mathbf{T}_i, \infty]$,

$$\underline{\mathbf{W}}_i^{\mathbf{A}_i, \mathbf{B}_i}(t) = \underline{\tilde{Z}}_i^{\mathbf{A}_i, \mathbf{B}_i}(t - \mathbf{T}_i).$$

Moreover, for $t > \tau$, we define the **rotated delayed extended oval trajectories**, $\underline{\tilde{\mathbf{V}}}_i(t) = (\tilde{\mathbf{v}}_i(t), \tilde{\mathbf{v}}_i(t))$ of the i 'th vehicle

$$(\tilde{\mathbf{v}}_i(t), \tilde{\mathbf{v}}_i(t)) = ROT_{\Theta_i} \left(\underline{\mathbf{W}}_i^{\mathbf{A}_i, \mathbf{B}_i}(t) \right), \quad (20)$$

where ROT_{Θ_i} is the rotation around the origin by Θ_i degrees and $\Theta_i \sim U(0, 2\pi)$ is chosen independently from each other.

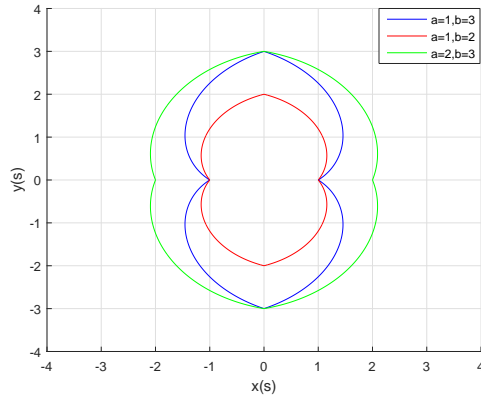


Fig. 7. Typical curves from the oval trajectory process.

An example of curves satisfying the Properties 1 and 2 of Definition 2 can be defined in the polar coordinates of the following form

$$X(s) = [q \cos(\frac{\pi}{2}s), q \sin(\frac{\pi}{2}s)], \quad s \in [0, 1], \quad (21)$$

where $q = a + (b - a)s$ and a and b are random variables with a two-dimensional PDF $f_{\mathbf{A}, \mathbf{B}}(a, b)$ that satisfies (17). Figure 7 shows a representation of (21).

Now let's state the following lemma which will be used later in the proof of Theorem 2.

Lemma 2. *Let $\mathbf{T} \sim U(0, \tau)$. Fix $a, b \in \mathbb{R}^+$, where without loss of generality $0 \leq a \leq b \leq \rho$ (since the case of $0 \leq b \leq a \leq \rho$ can be considered as the rotated version of the former), and consider an extended oval trajectory $\tilde{\mathbf{Z}}^{a,b}(t)$ as defined in Definition 2. For $t \in [T, \infty]$, define the delayed extended oval trajectory $\mathbf{W}^{a,b}(t)$ as $\mathbf{W}^{a,b}(t) = \tilde{\mathbf{Z}}^{a,b}(t - \mathbf{T})$. Then for any $t > \tau$, we have*

$$\|\mathbf{W}^{a,b}(t)\| \sim U(a, b).$$

Proof. We provide the proof for $0 \leq t \leq \frac{\tau}{4}$. The proof is similar for other values of t . Similar to the procedure developed for the proof of Theorem 1, let $u(t) = \|\tilde{\mathbf{Z}}^{a,b}(h^{-1}(t))\|$, $0 \leq t \leq \frac{\tau}{4}$

and $\|\underline{\mathbf{W}}^{a,b}(t)\| = u(t - \mathbf{T})$, where \mathbf{T} is a uniform random variable in the interval $(0, \tau)$. With these assumptions and using Lemma 1, we obtain

$$\begin{aligned} F_{\|\underline{\mathbf{W}}^{a,b}\|} &= \frac{4|\{0 \leq \beta \leq \frac{\tau}{4} : u(\beta) \leq r\}|}{\tau} \\ &= \frac{4|\{0 \leq \beta \leq \frac{\tau}{4} : \|\tilde{\underline{\mathbf{Z}}}^{a,b}(h^{-1}(\beta))\| \leq r\}|}{\tau}, \end{aligned} \quad (22)$$

where since $h(s)$ defined in (16) is a non-decreasing function of s , we can say that there exists a β_{\max} for which we have $\|\tilde{\underline{\mathbf{Z}}}^{a,b}(h^{-1}(\beta_{\max}))\| \leq r$. Hence, we get

$$F_{\|\underline{\mathbf{W}}^{a,b}\|} = \frac{4|[0, \beta_{\max}]|}{\tau} = \frac{4\beta_{\max}}{\tau}. \quad (23)$$

On the other hand, let $0 \leq \beta^* \leq \frac{\tau}{4}$, $\beta^* = \frac{\tau(r-a)}{4(b-a)}$ which means there exists a $s^* \in [0, 1]$ for which $\beta^* = h(s^*)$. Therefore, we have $h^{-1}(\beta^*) = h^{-1}(\beta_{\max})$ and since h is monotonic, we uniquely have $\beta^* = \beta_{\max}$. Finally we obtain the CDF of the distance between any point on the first quarter located on the curve $\underline{W}^{a,b}(t)$ and the origin as below

$$F_{\|\underline{\mathbf{W}}^{a,b}\|} = \frac{4|\{0 \leq \beta \leq \beta_{\max}\}|}{\tau} = \frac{4\beta_{\max}}{\tau} = \frac{r-a}{b-a}, \quad (24)$$

which is the CDF of a random variable distributed uniformly between a and b . \square

We are now ready to state Theorem 2:

Theorem 2. For all $t > \tau$, the instantaneous locations of the aerial vehicles on the rotated delayed extended oval trajectory, i.e., $\tilde{\underline{\mathbf{V}}}(t)$, form a uniform BPP in $B(\underline{O}, \rho)$.

Proof. Similar to the case of Theorem 1, since $\Theta_i \in (0, 2\pi)$ and $\mathbf{T}_i \in (0, \tau)$ are each chosen independently, we conclude that the points on the curves are independent. Now we can obtain the distribution of distances of the points on the rotated delayed extended oval trajectory $\tilde{\underline{\mathbf{V}}}_i(t)$ for $t \geq \tau$, $f_{\|\tilde{\underline{\mathbf{V}}}\|}(r)$ as below

$$f_{\|\tilde{\underline{\mathbf{V}}}\|}(r) \stackrel{(i)}{=} \int_a \int_b f_{\|\tilde{\underline{\mathbf{V}}}\|\mathbf{A},\mathbf{B}}(r|a, b) f_{\mathbf{A},\mathbf{B}}(a, b) da db$$

$$= \mathbb{E}_{\mathbf{A}, \mathbf{B}} [f_{\|\tilde{\mathbf{Y}}\|_{\mathbf{A}, \mathbf{B}}}(r|a, b)] \stackrel{\text{(ii)}}{=} \mathbb{E}_{\mathbf{A}, \mathbf{B}} \left[\frac{\mathbb{1}_{\mathbf{A} \leq r \leq \mathbf{B}}}{\mathbf{B} - \mathbf{A}} \right], \quad (25)$$

where (i) results from the law of total probability and (ii) comes from Lemma 2 where we showed that given a and b , the distribution of $\|\underline{\mathbf{W}}^{a,b}(t)\|$ is uniform in the interval (a, b) . Finally, according to (17) the last statement in (25) is equal to $\frac{2r}{\rho^2}$ and so we have $f_{\|\tilde{\mathbf{Y}}\|}(r) = \frac{2r}{\rho^2}$ which completes the proof. \square

In the following, we bring up two special cases of the oval trajectory processes.

2) *Ellipse and ring processes*: Assume that for the i^{th} ABS, we fix $\mathbf{B}_i = \rho$ and $f_{\mathbf{A}_i}(a) = \frac{2}{\rho^2}(\rho - a)$ and $0 \leq a \leq \rho$. Now, by setting $b = \mathbf{B}_i$ and $a = \mathbf{A}_i$ in (21), it reduces to an ellipse with semi-major axis \mathbf{B}_i and semi-minor axis \mathbf{A}_i . To show that it is an oval trajectory, we have to check out if (17) holds. To do so, we observe that

$$\begin{aligned} \mathbb{E}_{\mathbf{A}_i, \mathbf{B}_i} \left[\frac{\mathbb{1}_{\mathbf{A}_i \leq r \leq \mathbf{B}_i}}{\mathbf{B}_i - \mathbf{A}_i} \right] &= \mathbb{E}_{\mathbf{A}_i} \left[\frac{\mathbb{1}_{\mathbf{A}_i \leq r}}{\rho - \mathbf{A}_i} \right] = \int_0^r \frac{2}{\rho^2(\rho - a)}(\rho - a)da \\ &= \frac{2r}{\rho^2}, \quad 0 \leq r \leq \rho, \end{aligned} \quad (26)$$

which satisfies (17). We refer to this process as the *ellipse process*.

Another special case can be obtained by assuming \mathbf{B}_i to be a random variable with $f_{\mathbf{B}_i}(b) = \frac{2b}{\rho^2}$ and $\mathbf{A}_i = \mathbf{B}_i - \epsilon$ with probability 1. Again, with $a = b = \mathbf{B}_i$ which results in $q = \mathbf{B}_i$ in (21), this trajectory which henceforth called the *ring process*, represents a circle with the radius \mathbf{B}_i on which an ABS i turns around the center with a constant speed of $\mathbf{v}_{i, \text{ring}} = \frac{2\pi\mathbf{B}_i}{\tau}$. Such a constant speed is a major practical advantage over other members of the oval trajectory family as well as the spiral trajectory. Again, we investigate if (17) holds:

$$\begin{aligned} \mathbb{E}_{\mathbf{A}_i, \mathbf{B}_i} \left[\frac{\mathbb{1}_{\mathbf{A}_i \leq r \leq \mathbf{B}_i}}{\mathbf{B}_i - \mathbf{A}_i} \right] &= \frac{1}{\epsilon} \Pr(\mathbf{B}_i - \epsilon \leq r \leq \mathbf{B}_i) = \frac{1}{\epsilon} \int_r^{r+\epsilon} f_{\mathbf{B}_i}(b)db \\ &= \frac{2r + \epsilon}{\rho^2}, \end{aligned} \quad (27)$$

where as $\epsilon \rightarrow 0$, it converges to $\frac{2r}{\rho^2}$.

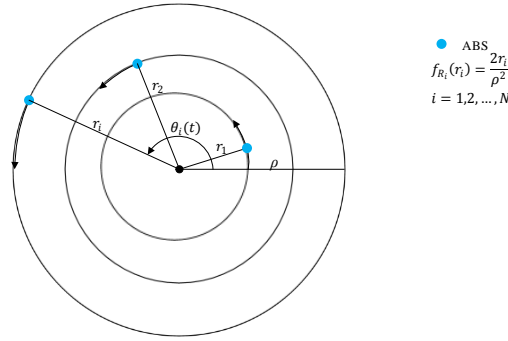


Fig. 8. An illustration of flying ABSs according to a ring trajectory process.

D. Deterministic Practical Trajectories for Moving ABSs

In this section, we provide two deterministic schemes corresponding to each of the two proposed stochastic trajectory families. We show that these deterministic trajectories have asymptotically the same statistical averages as their stochastic counterparts. To do so, we propose the following lemma which we then use it in the sequel.

Lemma 3. *Let $\mathbf{X} \in [a_x, b_x]$ be a continuous random variable with CDF $F_{\mathbf{X}}(x)$ and for $N \in \mathbb{N}$, let $x_i = F^{-1}\left(\frac{i}{N}\right)$, i.e., $F_{\mathbf{X}}(x_i) = \frac{i}{N}$. Also, let $g: \mathbb{R} \rightarrow \mathbb{R}$ be continuous. Then, we have:*

$$\mathbb{E}(g(\mathbf{X})) = \lim_{N \rightarrow \infty} \frac{1}{N} \sum_{i=1}^N g(x_i). \quad (28)$$

Proof.

$$\begin{aligned} \mathbb{E}(g(\mathbf{X})) &= \int_{\mathbb{R}} g(\mathbf{X}) dF_{\mathbf{X}}(x) \stackrel{(a)}{=} \lim_{N \rightarrow \infty} \sum_{i=1}^N g(x_i) [F_{\mathbf{X}}(x_{i+1}) - F_{\mathbf{X}}(x_i)] \\ &= \lim_{N \rightarrow \infty} \sum_{i=1}^N g(x_i) \left[\frac{i+1}{N} - \frac{i}{N} \right] = \lim_{N \rightarrow \infty} \frac{1}{N} \sum_{i=1}^N g(x_i). \end{aligned}$$

where (a) results from the continuity of g . □

Corollary 2. *Setting $x_i = F^{-1}\left(\frac{i-1}{N}\right)$ or $x_i = F^{-1}\left(\frac{i}{N+1}\right)$ one can obtain the same result.*

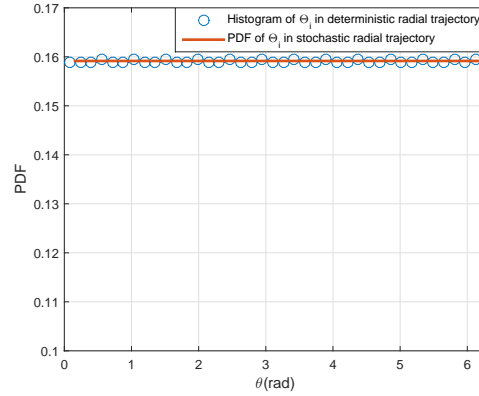


Fig. 9. Histogram of Θ_i in the radial deterministic model vs. the PDF of Θ_i in the radial trajectory process.

1) *Deterministic radial trajectory*: To design a deterministic trajectory counterpart for the radial process proposed in Section III-B2, according to the Lemma 3 and Corollary 2, we chose

$$\Theta_i \text{ and } T_i \text{ as} \quad \Theta_i = \frac{i-1}{N} 2\pi, \quad i = 1, 2, \dots, N, \quad (29)$$

and

$$T_i = \frac{i}{N+1} \tau, \quad i = 1, 2, \dots, N, \quad (30)$$

respectively. This results in that if again the ABSs follow (14), their distance will show the same statistical behavior as when they follow a radial trajectory process.

Figure 9 confirms that the histogram of Θ_i tends to a random variable uniformly distributed in $(0, 2\pi)$. The same result can be confirmed for T_i .

2) *Deterministic ring trajectory*: In the same way, according to Lemma 3 and Corollary 2, deterministic ring trajectory can be designed by choosing R_i 's according to

$$R_i = \sqrt{\frac{i}{N+1}} \rho, \quad (31)$$

and

$$T_i = \frac{i}{N} \tau. \quad (32)$$

Figure 10 confirms that the histogram of R_i tends to the random variable $\mathbf{R} \sim f_{\mathbf{R}}(r)$.

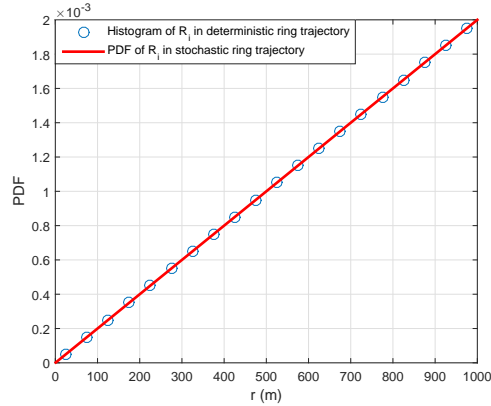


Fig. 10. Histogram of R_i in the deterministic model vs. the PDF of R_i in the ring trajectory process.

IV. SIMULATION RESULTS

In this section, we start with the verification of the coverage probability resulting from the proposed trajectory processes with analytical formulation (1). To generate Fig. 11, we set path-loss exponent $\alpha = 2.5$, Nakagami fading parameters $m = m_0 = 2$,⁴ $N = 5$, $\rho = 4$ km, $H = 200$ m and the interference is modeled similar to [11].⁵ Also the typical user (receiver) is 400 m away from the center.

Fig. 11 represents the coverage probability evaluation of the proposed system models as well as the one obtained analytically from Proposition 1. This figure shows the validity of our claim that the proposed system models provide the same coverage as the static case. This also holds to some extent for the deterministic system model.

⁴It is important to note that the altitude of the ABSs directly affects the coverage probability. This impact is already reflected in the considered channel path loss model similar to [11], [39], and [40].

⁵In the emerging aerial networks framework, the modeling of the air-to-ground channels is an active research area in 3GPP (currently being discussed in a number of technical reports and technical specifications) and in other platforms. It should be noted that, identifying the most appropriate channel model type is not the ultimate goal in this paper; rather, a channel model widely used in the literature is utilized as a means towards designing the ABS trajectory paths.

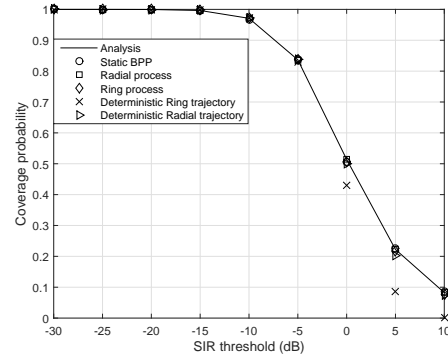


Fig. 11. Coverage probability of the proposed system models: simulation vs. analysis.

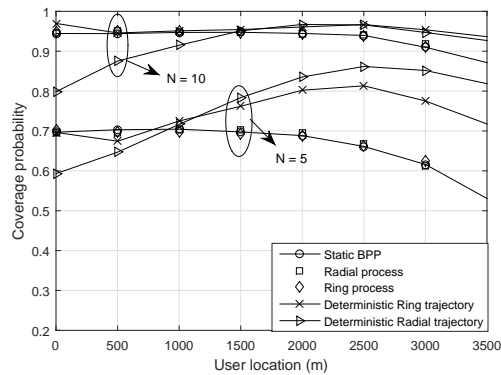


Fig. 12. Coverage probability vs. user location in the proposed processes in a network without interference.

Now let's assume that the bandwidth is divided orthogonally between the ABSs such that we do not experience any interference in the network. Fig. 12 shows the coverage in two scenarios of $N = 5$ and $N = 10$ where we set the SIR threshold β to be 0 dB. According to this figure, when $N = 10$, all the trajectories show a similar behavior to the static BPP network. However, with $N = 5$, the deterministic trajectories have a little different behavior since as the number of N decreases they can be no longer assumed to be modeled close to a BPP in each time snapshot. However, they can provide better coverage at the cell edge compared to the stochastic models since they benefit from regular arrangement. As can be seen, the performance improves

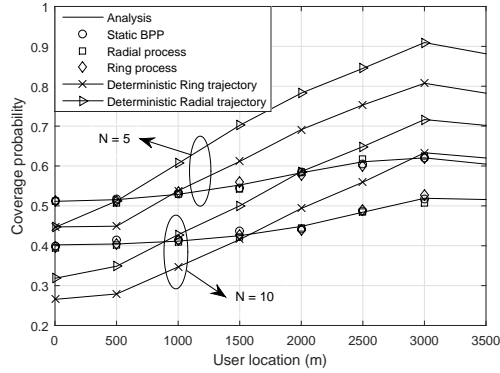


Fig. 13. Coverage probability vs. user location in the proposed processes in a network with interference.

in a dense setting.

If we assume that the bandwidth is shared among the ABSs, we have to consider the interference experienced by the user. Fig. 13 represents the coverage probability in this setup. As can be seen, both radial and ring processes provide the same coverage behavior as that of the static BPP case, while the performance for the deterministic scenarios is a bit different. It is interesting to note that in contrast to the interference-free case, a dense setting, i.e., increasing the number of ABSs (N) does not necessarily improve the coverage as it simultaneously increases the amount of interference.

As discussed in Section I, the most important benefit of deploying moving ABSs is the reduction of AFD, the simulation procedure of which is provided in the Appendix. In the next figures (Figures 14 and 15), we investigate the AFD for the 4 mobile scenarios and compare it with the AFD corresponding to the static case. To this end, the average velocity in ring and radial trajectory obtained by $\bar{v}_{\text{Ring}} = \frac{2\pi E(\mathbf{R})}{\tau}$ and $\bar{v}_{\text{radial}} = \frac{\rho}{\tau}$, respectively, is set to be 5 m/s which is a practical value. We keep the SIR threshold $\beta = 0$ dB. By these assumptions, we measure the received SIR at the receiver locations for an interval of 100 seconds. Fig. 14 compares the

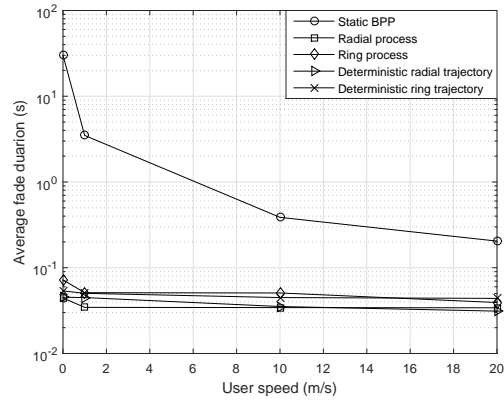


Fig. 14. Average fade duration with N=5 ABSs.

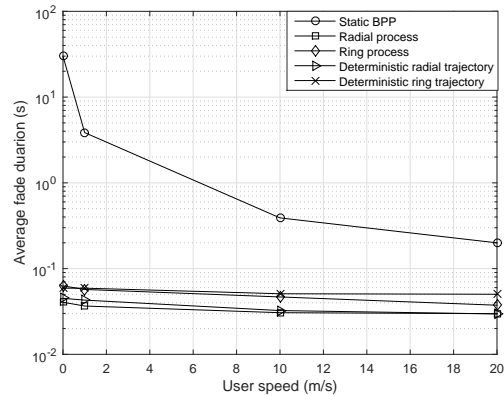


Fig. 15. Average fade duration with N=10 ABSs.

AFD of the conventional static case and that of the mobile case.

As can be seen, in all 4 cases we have significant improvement in AFD compared to the static case. For lower user speeds, the AFD of static case is too large and even unacceptable while for the mobile case, it is reduced to reasonable values. This improvement is between one to two orders of magnitude for walking/biking speeds. As the user speed increase, the difference between the AFD of static and moving ABS starts to decrease. Nevertheless, even for speeds as high as 20 m/s (50 miles/hour), the mobile case still significantly outperforms the static case.

V. CONCLUSION

In this paper, we designed a network of moving ABSs for which we can provide a fairly uniform coverage probability to the users within a cell while significantly improving the average fade duration experience for the users. This was achieved by designing stochastic trajectory processes that if according to which the ABSs move, at any snapshot the ABSs can still be modeled as a BPP. We introduced two families of such processes, namely spiral and oval processes and analytically proved the uniformity. We then focused on 2 special cases of such processes, namely, radial and ring processes, and showed that the AFD is reduced about two orders of magnitude with respect to the static case. Finally, by introducing deterministic counterparts of the proposed radial and ring processes and showing that similar coverage and AFD as the stochastic case are achievable, we have in fact proposed a practical and feasible scenario for networks of moving ABSs that can provide the necessary coverage while simultaneously providing the benefits of mobility.

APPENDIX

Simulation Procedure of AFD: To simulate the AFD, we consider independent fading coefficients every time the distance between the user and the associated ABS changes more than $\lambda/2$ where λ , the wavelength, is defined as $\lambda = \frac{c}{f_c}$. In this equation, c is the light speed and f_c is the carrier frequency. To precisely capture such changes, the time instant quantization Δt has to be small enough depending on the relative speed V between the ABS and user. Let $\Delta x = V\Delta t$ be the change in the distance of the user and its associated ABS in Δt seconds. We have to choose Δt such that Δx is sufficiently smaller than $\lambda/2$. The smaller the Δt is, the more accurate the simulation setup will be at the expense of larger simulation complexity. In our case, we assume $f_c = 1\text{ GHz}$, for which $\lambda/2 = 15\text{ cm}$. Accordingly, we have set $\Delta t = 1\text{ ms}$. Doing so, at relative speeds as large as 30 m/s (100 Km/h), we have at least 5 time samples which

observe a fixed fading coefficient. Now we generate the coefficients according the considered distribution (here, Nakagami) and at each time instant, we record the associated gain for the whole period of measurement (here $T = 100\text{ s}$) for any user-ABS pair. Now based on the required SIR threshold, we find blocks of time instants for which all the associated gains are below the given SIR threshold and record their time length. Then we average over such lengths to obtain the AFD. To be sure of the accuracy of the chosen Δt , we have examined smaller values for Δt (i.e., 0.1 ms) at the expense of increasing the simulation complexity one order of magnitude and the AFD results were almost the same. Therefore, for the speeds up to 100 Km/h , time instants around 1 ms seem to be sufficiently small for simulating AFD.

REFERENCES

- [1] S. Enayati, H. Saeedi, and H. Pishro-Nik, "Trajectory processes that preserve uniformity: A stochastic geometry approach," *Accepted in IEEE International Symposium on Information Theory (ISIT)*, July 2018, Vail, CO, USA.
- [2] N. Goddemeier, K. Daniel, and C. Wietfeld, "Role-based connectivity management with realistic air-to-ground channels for cooperative UAVs," *IEEE Journal on Selected Areas in Communications*, vol. 30, no. 5, pp. 951–963, Jun. 2012.
- [3] S. Hayat, E. Yanmaz, and R. Muzaffar, "Survey on unmanned aerial vehicle networks for civil applications: a communications viewpoint," *IEEE Communications Surveys & Tutorials*, vol. 18, no. 4, pp. 2624–2661, 2016.
- [4] L. Gupta, R. Jain, and G. Vaszkun, "Survey of important issues in UAV communication networks," *IEEE Communications Surveys & Tutorials*, vol. 18, no. 2, pp. 1123–1152, 2015.
- [5] F. Ono, H. Ochiai, and R. Miura, "A wireless relay network based on unmanned aircraft system with rate optimization," *IEEE Transactions on Wireless Communications*, vol. 15, no. 11, pp. 7699–7708, Nov. 2016.
- [6] Y. Zeng and R. Zhang, "Energy-efficient UAV communication with trajectory optimization," *IEEE Transactions on Wireless Communications*, vol. 16, no. 6, pp. 3747–3760, Jun. 2017.
- [7] A. Filippone, *Flight Performance of Fixed and Rotary Wing Aircraft*. American Institute of Aeronautics & Ast., 2006.
- [8] M. Guizani, *Wireless Communications Systems and Networks*. Kluwer Academic Publishers, 2004.
- [9] M. Mozaffari, W. Saad, M. Bennis, and M. Debbah, "Unmanned aerial vehicle with underlaid device-to-device communications: Performance and tradeoffs," *IEEE Transactions on Wireless Communications*, vol. 15, no. 6, pp. 3949–3963, Jun. 2016.

- [10] J. Lyu, Y. Zeng, and R. Zhang, "Cyclical multiple access in UAV-aided communications: A throughput-delay tradeoff," *IEEE Wireless Communications Letters*, vol. 5, no. 6, pp. 600–603, Dec. 2016.
- [11] V. V. Chetlur and H. S. Dhillon, "Downlink coverage analysis for a finite 3D wireless network of unmanned aerial vehicles," *IEEE Transactions on Communications*, vol. 65, no. 10, pp. 4543–4558, Oct. 2017.
- [12] Y. Zeng, R. Zhang, and T. J. Lim, "Throughput maximization for UAV-enabled mobile relaying systems," *IEEE Transactions on Communications*, vol. 64, no. 12, pp. 4983–4996, Dec. 2016.
- [13] C. Zhang and W. Zhang, "Spectrum sharing for drone networks," *IEEE Journal on Selected Areas in Communications*, vol. 35, no. 1, pp. 136–144, Jan. 2017.
- [14] M. Mozaffari, W. Saad, M. Bennis, and M. Debbah, "Drone small cells in the clouds: Design, deployment and performance analysis," in *IEEE Global Communications Conference (GLOBECOM)*, San Diego, CA, USA, Dec. 2015, pp. 1–6.
- [15] J. Lyu, Y. Zeng, R. Zhang, and T. J. Lim, "Placement optimization of UAV-mounted mobile base stations," *IEEE Communications Letters*, vol. 21, no. 3, pp. 604–607, Mar. 2017.
- [16] E. Kalantari, H. Yanikomeroglu, and A. Yongacoglu, "On the number and 3D placement of drone base stations in wireless cellular networks," in *Proc. of IEEE Vehicular Technology Conference (VTC-Fall)*, Montreal, QC, Canada, Sep. 2016.
- [17] M. Mozaffari, W. Saad, M. Bennis, and M. Debbah, "Efficient deployment of multiple unmanned aerial vehicles for optimal wireless coverage," *IEEE Communications Letters*, vol. 20, no. 8, pp. 1647–1650, Aug. 2016.
- [18] —, "Optimal transport theory for power-efficient deployment of unmanned aerial vehicles," in *Proc. of IEEE International Conference on Communications*, Kuala Lumpur, Malaysia, May 2016, pp. 1–6.
- [19] —, "Optimal transport theory for cell association in UAV-enabled cellular networks," *IEEE Communications Letters*, vol. 21, no. 9, pp. 2053–2056, Sep. 2017.
- [20] R. Yaliniz, A. El-Keyi, and H. Yanikomeroglu, "Efficient 3-D placement of an aerial base station in next generation cellular networks," in *Proc. of IEEE International Conference on Communications*, Kuala Lumpur, Malaysia, May 2016, pp. 1–5.
- [21] M. Mozaffari, W. Saad, M. Bennis, and M. Debbah, "Mobile unmanned aerial vehicles (UAVs) for energy-efficient internet of things communications," *IEEE Transactions on Communications*, vol. 16, no. 11, pp. 7574–7589, Nov. 2017.
- [22] Q. Wu, Y. Zeng, and R. Zhang, "Joint trajectory and communication design for uav-enabled multiple access," in *IEEE Global Communications Conference (GLOBECOM)*. IEEE, Singapore, Singapore, Dec. 2017, pp. 1–6.
- [23] —, "Joint trajectory and communication design for multi-UAV enabled wireless networks," *IEEE Transactions on Wireless Communications*, vol. 17, no. 3, pp. 2109–2121, March 2018.
- [24] J. Lyu, Y. Zeng, and R. Zhang, "UAV-aided offloading for cellular hotspot," *IEEE Transactions on Wireless Communications*, vol. 17, no. 6, pp. 3988 – 4001, Jun. 2018.
- [25] W. Feng, J. Wang, Y. Chen, X. Wang, N. Ge, and J. Lu, "UAV-aided MIMO communications for 5G internet of things,"

- IEEE Internet of Things Journal*, Early Access 2018.
- [26] B. Galkin, J. Kibilda, and L. A. DaSilva, "A stochastic geometry model of backhaul and user coverage in urban UAV networks," *arXiv preprint arXiv:1710.03701*, 2017.
- [27] Y. Cai, F. Cui, Q. Shi, M. Zhao, and G. Li, "Dual-UAV enabled secure communications: joint trajectory design and user scheduling," *IEEE Journal on Selected Areas in Communications*, vol. 36, no. 9, pp. 1972 – 1985, Sep. 2018.
- [28] Q. Wang, Z. Chen, H. Li, and S. Li, "Joint power and trajectory design for physical-layer secrecy in the UAV-aided mobile relaying system," *IEEE Access*, vol. 6, pp. 62 849–62 855, 2018.
- [29] X. Jiang, Z. Wu, Z. Yin, and Z. Yang, "Joint power and trajectory design for UAV-relayed wireless systems," *IEEE Wireless Communications Letters*, Early Access, 2018.
- [30] L. Xie, J. Xu, and R. Zhang, "Throughput maximization for UAV-enabled wireless powered communication networks," *IEEE Internet of Things Journal*, Early Access, 2018.
- [31] X. Zhou, S. Yan, J. Hu, J. Sun, J. Li, and F. Shu, "Joint optimization of a UAVs trajectory and transmit power for covert communications," *arXiv preprint arXiv:1812.00583*, Dec. 2018.
- [32] Y. Zeng, X. Xu, and R. Zhang, "Trajectory design for completion time minimization in UAV-enabled multicasting," *IEEE Transactions on Wireless Communications*, vol. 17, no. 4, pp. 2233–2246, Apr. 2018.
- [33] G. Zhang, H. Yan, Y. Zeng, M. Cui, and Y. Liu, "Trajectory optimization and power allocation for multi-hop UAV relaying communications," *IEEE Access*, vol. 6, pp. 48 566–48 576, Aug. 2018.
- [34] S. Eom, H. Lee, J. Park, and I. Lee, "UAV-aided wireless communication designs with propulsion energy limitations," *arXiv preprint arXiv:1801.02782*, 2018.
- [35] M. Haenggi, J. G. Andrews, F. Baccelli, O. Dousse, and M. Franceschetti, "Stochastic geometry and random graphs for the analysis and design of wireless networks," *IEEE Journal on Selected Areas in Communications*, vol. 27, no. 7, Sep. 2009.
- [36] J. G. Andrews, A. K. Gupta, and H. S. Dhillon, "A primer on cellular network analysis using stochastic geometry," *arXiv preprint arXiv:1604.03183*, 2016.
- [37] H. ElSawy, A. Sultan-Salem, M.-S. Alouini, and M. Z. Win, "Modeling and analysis of cellular networks using stochastic geometry: A tutorial," *IEEE Communications Surveys & Tutorials*, vol. 19, no. 1, pp. 167–203, Firstquarter 2017.
- [38] M. Haenggi, *Stochastic Geometry for Wireless Networks*. Cambridge University Press, 2012.
- [39] I. Atzeni, J. Arnau, and M. Kountouris, "Downlink cellular network analysis with los/nlos propagation and elevated base stations," *IEEE Transactions on Wireless Communications*, vol. 17, no. 1, pp. 142–156, Jan. 2018.
- [40] Y. Zhu, G. Zheng, and M. Fitch, "Secrecy rate analysis of UAV-enabled mmwave networks using matern hardcore point processes," *IEEE Journal on Selected Areas in Communications*, vol. 36, no. 7, pp. 1397 – 1409, Jul. 2018.